Influence of System Size in Molecular Dynamics Simulations of Gas Permeation in Glassy Polymers

Sylvie Neyertz* and David Brown

Laboratoire Matériaux Organiques à Propriétés Spécifiques (LMOPS), UMR CNRS 5041, Université de Savoie, Bât. IUT, 73376 Le Bourget-du-Lac Cedex, France

Received July 22, 2004; Revised Manuscript Received October 4, 2004

ABSTRACT: The dependence of gas permeation on system size in glassy polymers has been tested by creating several models containing different numbers of molecules of the same chain length for the ODPA−ODA homopolyimide and by subsequently determining the permeation characteristics of helium. Eight "standard size" 4150-atom, a 6225-atom, and a much more expensive computationally 56025-atom systems were generated using hybrid pivot Monte Carlo (PMC)−molecular dynamics (MD) single-chain sampling. Following the careful relaxation of the polyimide matrices, helium atoms were then inserted into these systems, and MD simulations were carried out at the same applied external conditions of constant temperature and pressure tensor. Average densities for the pure matrices all fell within 0.7% of the experimental value. Energetic and structural properties as well as solubilities and characterization of the void space were also found to be number independent, thus showing that the preparation procedure gives reproducible and reliable results. Helium diffusion was analyzed over periods up to 20 ns using different approaches, such as observation of the individual trajectories, mean-square displacements, distributions of penetrant displacements components, and van Hove correlation functions. No number dependence could be detected, whether the gas molecules were in the anomalous or in the Fickian regime.

1. Introduction

Polyimides are high-performance macromolecules, which combine excellent mechanical characteristics with good thermal, chemical, and long-term stabilities.[1] They exhibit high gas selectivities and can thus be used as dense membranes for gas separation, e.g., for separating oxygen or nitrogen from air or for purifying natural gas.[2] The choice of their basic dianhydride and diamine monomers can be fine-tuned in order to lead to a large variety of flexibilities, mobilities, and structural packings,[1−3] which in turn will be directly linked to the selectivity and permeability of the resulting polyimide membrane. However, it should be stressed that the chemical structure is only one of the determinants of the permeation properties.[4] It is now well-known that the membrane processing and postprocessing conditions are also key parameters for improving permeabilities while keeping high selectivities.[5,6]

There has been much experimental effort dedicated toward identifying and understanding the multiple factors at the basis of good permeation properties,[1,2,4] and molecular dynamics (MD) simulations[7] have also been used to complement experimental evidence by providing atomistic models of the transport of small gas molecules in polymide matrices. First investigations included the introduction of a limited number of CO_2, O_2, or N_2 penetrants in several polyimide matrices.[8,9] It was also attempted to correlate energy-minimized molecular models of pure polyimides with experimentally measured permeabilities.[10] However, the most extensive work to date is that of Hofmann, Heuchel, and co-workers.[11−15] These authors first studied the diffusion mechanisms of H_2, O_2, and N_2 in a fluorinated 6FDA-polyimide, which was singled out for its high gas permeabilities,[16] and in a trimethylphenylene-modified neighboring structure.[11] They were able to obtain good diffusivities and solubilities and to reveal qualitative key differences in gas mobility through flexible rubbery and stiff glassy polymers.[12−14] More recently, they have extended their work to O_2, N_2, CH_4, and CO_2 in a series of nine other polyimides based on the 6FDA dianhydride and in PMDA−ODA.[15,17] With improved equilibration strategies and a better force field, they could predict selectivity values for O_2/N_2 separation and identify the key role of a methyl group, in an ortho position to the imide group on the aromatic diamine moieties, toward attaining high O_2 permeabilities.[15,17]

The present work follows a recent series of MD simulations, which were undertaken on five closely related copolyimides in their pure state.[18] The copolyimides were based on different dianhydrides and diamines, among which the flexible 4,4′-oxydiphthalic dianhydride moiety (ODPA) and the 4,4′-oxydi(phenylamine) (ODA) diamine. The features of the model chains were chosen in order to correspond as closely as possible to experimental data.[19−21] The preparation procedure for the chain configurations and the force field used were subsequently validated by experimental results for densities, solubility parameters, d spacings, color indices, and free volume fractions.[18] The discrepancy between simulated and experimental densities was found to be small in all cases;[18] indeed, they agreed within 0.7% (0.009 g cm^{-3}) for the (ODPA−ODA) homopolyimide.

Following the synthesis and modeling of the aforementioned copolyimides, preliminary investigations were carried out in order to characterize their permeation properties with respect to He, O_2, and N_2 gas. Force-field parameters for the gas molecules[22,23] were also carefully validated with respect to their experimental solid or liquid densities (the differences being <1%). Despite these precautions, the calculated gas diffusion coefficients were found to be systematically larger than the measured ones.[19] In the case of helium, for example,

* Corresponding author. E-mail Sylvie.Neyertz@univ-savoie.fr.

10.1021/ma048500q CCC: $27.50 © 2004 American Chemical Society
Published on Web 11/26/2004

this typically amounted to a factor of at least 25.[19] Although the numerous difficulties encountered when comparing experimental to simulated data in the case of polyimide membranes have been pointed out by Heuchel et al.,[17] our main concern was the systematic trend in overestimating diffusivity in our models, regardless of the thorough preparation of the pure matrices.[18]

To explain these discrepancies, one of the suggestions was that the original 6500-atom systems[18] were maybe too small (which could lead to artificially large diffusion coefficients due to percolating periodic "channels"[14]), albeit fairly typical of such simulations.[15,17] The main aim of this work is thus to test the dependence of gas diffusion on the system size. A series of ODPA−ODA homopolyimide systems are prepared and the permeation characteristics subsequently determined. It should be noted that finite size effects are not a new preoccupation[24−26] and that, in glassy polymers, the simulation size effect of gas diffusion has already been investigated in different ways. Diffusion coefficients of He in polycarbonate, obtained using transition state theory (TSA), were reported to differ by 30% in a ∼30 or ∼50 Å side simulation box.[27] Bond-fluctuation model Monte Carlo simulations of penetrant particles in frozen polymer matrices showed that both their diffusion coefficients and the extent of the anomalous regime were dependent on the size of the simulation box.[28] Weber and Paul correlated penetrant diffusion in these static structures to percolating free volume clusters.[28] Cuthbert and Wagner et al.[29,30] carried out MD simulations of gas diffusion in glassy polystyrene (PS) and polypropylene (PP) with different box sizes. Several polymer chain lengths were considered (from 40 to 364 monomers for all-atomistic PS[29] and from 125 to 2197 monomers for united-atom PP[30]), i.e., from ∼375 up to ∼6600 atoms per simulation box at a fixed density. The initial configuration of the one parent chain was generated with a Gaussian lattice algorithm,[31] and different sizes of penetrant gas molecules were used.[29,30] Solubility was found to be chain length dependent for the larger penetrants, and this was attributed to a bias against the formation of large cavities in the smallest systems, although gas diffusion was virtually unaffected.[29,30] However, the authors did not report the pressures in their systems, which are expected to fall as the chain length increases at constant density. So, in a way, a special constraint was added in these simulations by forcing the different chain lengths to adopt the same density. Boshoff et al.[32] reported related MD simulations of He motion in frozen united-atom PP filled boxes (ranging from 250 to 2662 monomers), which led to the diffusion mechanism being altered from an activated process with dynamic jumps between fluctuating channels to hindered kinetic motion in a percolated amorphous pore network. Their results were consistent with those of Weber and Paul,[28] i.e., a clear size dependence of diffusivity on simulation box size.[32]

Here, we do not study system size dependence using a variety of chain lengths[29,30,32] but instead create several models containing different numbers of molecules of the *same* chain length for the ODPA−ODA homopolyimide. These systems are then simulated at the same applied external conditions of constant temperature and constant pressure tensor (NPT). Eight 4150-atom, one 6225-atom, i.e., the upper limit of the work of Cuthbert et al.[29,30] as well as Boshoff et al.,[32]

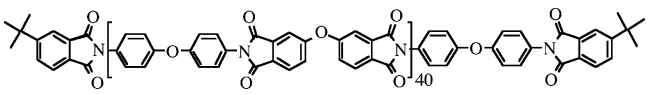

Figure 1. ODPA−ODA homopolyimide chain structure as determined from ^{1}H NMR characterization.[19,20]

and a much larger 56025-atom system were generated and relaxed with our validated polyimide potential.[18] Helium was then inserted into these different size models, since its kinetic diameter is much smaller than O_2 or N_2 and its permeability in polyimides is always much higher.[33−36] As expected, the 56025-atom model of a glassy polymer turned out to be extremely expensive in terms of computer time, which explains why this basic check is rarely carried out.

The computational details of all models are given in section 2, while the results are presented and discussed in section 3.

2. Computational Details

All simulations were performed using the *gmq* program[37] on the SGi ORIGIN 3800 and the IBM SP of the CINES (Montpellier, France), the IBM Regatta of the IDRIS (Orsay, France) supercomputing centers as well as on local SGi machines and a COMPAQ DS20E at the University of Savoie (Le Bourget-du-Lac, France). When using the parallel form of the MD code, *ddgmq*, simulation boxes were decomposed into $2 \times 2 \times 2 = 8$ domains each.

2.1. Chemical Structures. The basic model used here for the ODPA−ODA homopolyimide chains (Figure 1) is identical to that described in ref 18. As determined by ^{1}H NMR characterization,[19,20] chains consisting of 40 (dianhydride−diamine) units and terminated at both ends by a 4-*tert*-butylphthalic anhydride (PAtBu) were created using equilibrium bond lengths, bend, and dihedral angles.[38] The total number of atoms per ODPA−ODA chain was 2075. Helium was modeled as a single atom.

2.2. Potential. The functional form of the force field describing the potential energy of a system in the *gmq* programs has also been presented in detail elsewhere.[18,37] For the polyimides, the specific intramolecular terms consist of angle bending and out-of-plane deformations as well as torsional motions around dihedral angles, while high-frequency bond stretching modes are removed[39] to allow for the use of a reasonable time step, i.e., 1 fs in all simulations reported here.

Atoms belonging to the same chain (but separated by more than two bonds) and atoms belonging to different molecules also interact through the so-called "nonbonded" potentials. In the preparation phase of all pure polyimide systems,[18] the Lennard-Jones (LJ) form of the van der Waals potential between two atoms, U_{LJ}, was used:

$$U_{LJ}(r) = 4\epsilon((\sigma/r)^{12} - (\sigma/r)^6) \qquad (1)$$

with r being the distance between atoms i and j, ϵ the well depth of the potential, and σ the distance at which the potential is zero for atoms i and j. When atom types i and j are different, the ϵ_{ij} and σ_{ij} cross-terms are obtained from the geometric mean of ϵ_{ii} and ϵ_{jj} and from the arithmetic mean of σ_{ii} and σ_{jj}. The electrostatic

interactions were described by the Coulombic potential, U_{coul}:

$$U_{coul}(r) = q_i q_j / 4\pi\epsilon_0 r \quad (2)$$

with q_i and q_j being charges on atoms i and j, respectively, and ϵ_0 being the vacuum permittivity. The long-range effects of the electrostatic potential were taken into account by the Ewald summation method[40,41] in order to perform the infinite sum of partial charges distributed in a periodic system. Parameters for the polyimides came from the TRIPOS 5.2 force field,[38] with the exception of the partial charges which were obtained from ab initio calculations.[18]

Following the preparation of the polyimide matrices, it became clear that continuing to use the full aforementioned potential for the polyimide + gas models would rapidly become prohibitive in terms of computational costs, especially for the largest system. An alternative to MD simulations is the Gusev−Suter transition state theory (TST),[27] which is used by Heuchel and Hofmann et al. for their polyimide models[11−15,17] and allows far longer times to be attained (see e.g. Figure 1 of ref 17). However, one of the assumptions underlying the TST method is that the polymer packing does not undergo structural relaxations, and in view of the reported results on size effects (see the Introduction), this would bring an extra variable to the problem. As has been pointed out by Cuthbert et al.,[30] we are interested in the relative diffusion characteristics of the penetrants in different size matrices, and thus, the most important point is that the various systems are consistent with each other. Consequently, in that phase of the work, the "nonbonded" potentials were replaced by a much faster form of the excluded-volume effect in terms of calculation, the Weeks−Chandler−Andersen (WCA) potential, U_{WCA}, to be able to increase simulation run time and reach the Einstein limit for diffusion:

$$U_{WCA}(r) = 4\epsilon((\sigma/r)^{12} - (\sigma/r)^6) + \epsilon \qquad \text{when } r \le 2^{1/6}\sigma \quad (3a)$$

$$U_{WCA}(r) = 0 \text{ when} \qquad r > 2^{1/6}\sigma \quad (3b)$$

The $\sigma_{ii} = 2.6282$ Å and the $\epsilon_{ii}/k_B = 6.030$ K parameters for helium were derived from Lee et al.[42]

2.3. Preparation of Dense Polyimide Packing Models. As explained elsewhere,[18,43−49] our initial configuration generation procedure is a single-chain sampling technique, based on pivot Monte Carlo (PMC) moves[50] for rotatable torsions with standard molecular dynamics algorithms for exploring the various oscillatory modes of the chains. The Metropolis acceptance criteria[51] for Monte Carlo moves is directly linked to the changes in the "local energy", i.e., the assumption by Flory[52] that chain configurations in the melt can be described by considering only a certain number of near-neighbor intramolecular interactions. The aim of this preparation procedure is to produce samples directly at the density desired with the chains having conformations characteristic of the equilibrium melt at the required temperature.[44] It is worth noting that, prior to using this generation procedure for a given polymer, chain configurations obtained using hybrid PMC−MD single-chain sampling are systematically validated with respect to those in the corresponding bulk melts for relatively short chains.[43−49] Indeed, only small chain lengths can be totally decorrelated using MD on its own, which ensures that they are truly independent of their starting structures.

The application of the hybrid PMC−MD single-chain sampling method to the polyimide under study has been described in detail previously.[18,49] The sampling is carried out in the melt at 700 K, well above the experimental glass-transition temperature of the ODPA−ODA homopolyimide.[19] At this temperature, configurational decorrelation for polyimides has been found to occur within 20−50 ps sampling.[18] PMC moves on significant torsions are attempted every 100 MD steps of 1 fs for typically 150 ps, while the optimal number of bonds to consider in the local energy approximation is four.[49]

To assess the effect of the "nonbonded" potentials on the configurations, 5 ns runs were attempted for a single ODPA−ODA 40-unit chain using different parts of the "nonbonded" potentials. The root-mean-square radii of gyration, $(\langle S^2 \rangle)^{1/2}$, were found to be respectively 58.4 Å using U_{LJ} and U_{coul}, 62.5 Å using only U_{LJ}, and 62.0 Å using U_{WCA} on its own. In all cases, the square radii of gyration and square end-to-end distances distributions overlapped well (results not shown). ODPA−ODA chain configurations are thus mostly governed by the excluded-volume repulsive interactions, and the much faster Weeks−Chandler−Andersen potential, used in the polyimide + gas production runs, obviously does not disrupt the polyimide configurations.

The composition of the systems under study is shown in Table 1. Three different simulation system sizes were considered: the first consisted of two uncorrelated ODPA−ODA chains, i.e., 4150 atoms, the second of three uncorrelated chains, i.e., 6225 atoms, and the third of 27 uncorrelated chains, i.e., a total of 56025 atoms. As shown in Table 1, all these matrices will be referred to in the remaining part of this paper by their number of polyimide atoms. Eight independent systems were prepared for the 4150-atom size, while both 6225-atom and 56025-atom sizes were prepared just once.

Following the generation procedure, the required numbers of chains for a given size (see Table 1) were randomly reoriented and distributed in a periodic cubic MD box corresponding to the experimental density, i.e., 1.368 g cm^{-3}.[18] Periodic boundary conditions were applied in all three dimensions. "Phantom" carbon atoms were then introduced at the center of each cyclic group and connected to their respective ring atoms through flexible bonds with a force constant of 300 kg s^{-2}. These phantom atoms avoid the unphysical trapping of bonds in the rings upon introduction of the excluded volume. Indeed, the problems of unwanted catenation and spearing events have also been reported for other polyimides by Heuchel, Hofmann, and coworkers.[11−15,17] These authors chose another approach by inserting obstacle molecules such as methanol prior to polymer packing.[15,17,53]

The introduction of the full potential has to be carried out progressively in order to remove high-energy overlaps while maintaining the carefully prepared configurations. Short constant-volume (NVT) MD simulations of the systems were then performed with the bonded interactions and constraints switched on. Over the first 10 ps, the excluded-volume potential was progressively scaled by a factor varying from 0 to 1 with a rate of 0.1 ps^{-1}. Velocities were rescaled at each time step to remove the large amount of heat generated. Phantom atoms were then removed, and electrostatic interactions

Table 1. Composition and Acronyms of the ODPA−ODA Models under Study[a]

acronym	no. of polyimide chains	no. of helium atoms	no. of independent polyimide matrices	no. of independent gas-starting positions per system	production time for the polyimide + gas simulations/ps
4150-atom	2	17	8	1	20000
6225-atom	3	25	1	4	8000
56025-atom	27	225	1	1	8000

[a] The acronyms refer to the actual number of polyimide atoms in the simulation boxes.

were switched on. Within the restrictions on the domain decomposition algorithm of the parallel code[37,54,55] and acceptable CPU costs,[56] the optimal convergence of the Ewald sum for the 4150-atom and 6225-atom sizes was obtained using $\alpha = 0.30$ Å^{-1} and $K_{max} = 12$, while the real-space potential was truncated at 8.5 Å. In the 56025-atom box, these parameters were instead $\alpha = 0.20$ Å^{-1} and $K_{max} = 10$, and the cutoff for the real-space potential was set at 10.8 Å. In all cases, the Lennard-Jones potential was truncated at the same distance as the real-space potential, and long-range corrections to the energy and the pressure were calculated on the basis of the radial distribution functions being equal to unity beyond the cutoff.[7]

Each system was allowed to further relax at 700 K for about 200 ps in order to eliminate local hot spots and to come to thermal equilibrium. The temperature was maintained through loose coupling to a heat bath[57] with a coupling constant of 0.1 ps. It was progressively cooled toward its target temperature of 300 K at a rate of -1 K ps^{-1}. It was then switched to constant-pressure (NPT) conditions, in which the on-diagonal and off-diagonal components of the pressure tensor are maintained at ∼1 and ∼0 bar, respectively, by loose coupling with a coupling constant of 5 ps [58] and run for 200 ps at ∼300 K until the box size and shape settled around a constant value. To confirm that the systems would truly relax toward their actual density, an additional high-pressure (25000 bar) and high-temperature (1000 K) NVT annealing procedure was carried out for 200 ps, and the system was once again allowed to relax toward its equilibrium state at 300 K. The criterion for equilibration was that of Suter and co-workers for glassy polymers,[59−61] i.e., the absence of any drifts in density larger than 3×10^{-4} g cm^{-3} ps^{-1} during the last 100 ps of the equilibration procedure. A production run was carried out over 500 ps, during which configurations were stored at 10 ps intervals and thermodynamic and conformational data every 1 ps for postanalysis.

2.4. Polyimide−Helium Simulations. All 10 ODPA−ODA systems were used as matrices for He insertion, with the number of inserted gas molecules being proportional to the number of polymer molecules. Preliminary calculations based on the probability of insertion for He gas molecules (see later), the volume of the 56025-atom system simulation box, and the experimentally imposed pressure of 3 bar [19] showed that it would amount to less than four He molecules to be inserted into the 56025-atom matrix if one were to mimic exactly the experimental conditions. In addition, there would be less than one gas molecule in the 4150-atom and 6225-atom systems. To both improve the statistics and remain consistent with respect to the probability of insertion of He, it has thus proven necessary to set the number of gas molecules inserted into the polyimide matrix and adjust the external pressure P accordingly. A reasonable compromise was found with 17 He molecules in the 4150-atom sizes, 25 He molecules in the 6225-atom size, and 225 He molecules in the much larger 56025-atom size. From an estimate of the solubility, obtained using Widom's method[62] of inserting one gas molecule into a pure polyimide matrix, this would correspond to an external pressure of 180 bar, assuming Henry's law to be valid. In the medium size-system (6225 atoms), statistics were improved by preparing four separate polyimide + gas systems with different starting positions for the helium molecules. As far as diffusion is concerned, we also carried out a simulation of the 6225-atom size with five He molecules instead of 25 and found that the diffusion coefficient was the same within the, inevitably larger, error bars. However, we do not report this aspect in the present paper since its goal is to compare the three different system sizes under the same conditions, including the same He concentration.

For gas insertion, we used the same procedure as that described in an earlier investigation of the effect of water molecules on polyimide oligomers.[63] A box of helium of the same size as the corresponding ODPA−ODA model is prepared at a temperature of 300 K and at a density of ∼1 g cm^{-3}. Both boxes are then superimposed, and the required number of He atoms is added by selecting those which overlap least with the polyimide atoms. In this way, high overlap energies which could result from random insertions are avoided, and the initial gas-chain repulsions are reduced as much as possible. To avoid having the same helium starting positions for the four different simulations based on the 6225-atom matrix, different criteria for defining the overlaps were used for each of these systems. However, as was pointed out in ref 63, we suspect that, for very mobile penetrants such as He, this method gives similar results to a completely random insertion.

The polymer + helium systems were then simulated at ∼300 K with the polyimide intramolecular potentials[18] and the WCA form (eq 3) for the "nonbonded" terms until the density settled around a constant value, applying the same criterion for equilibration than above. The cutoff for the WCA potential was defined as given in eq 3b. However, since the WCA potential is purely repulsive, running at constant pressure will lead to an ever-expanding simulation box. To remove this artifact, the 6225-atom polyimide + gas system was briefly run with the full "nonbonded" potential, i.e., using U_{LJ} and U_{coul} instead of U_{WCA}. The relaxed system was then subjected to a constant-volume NVT run with U_{WCA} only, and the resulting pressure was found to be ∼8650 bar. All ODPA−ODA + gas systems were thus switched to constant-pressure (NPT) conditions, in which the on-diagonal and off-diagonal components of the pressure tensor were maintained at ∼8650 and ∼0 bar, respectively, by loose coupling with a coupling constant of 5 ps.[58] As will be shown later, this estimation keeps densities in good agreement with experimental evidence. All other parameters were similar to those given in section 2.3.

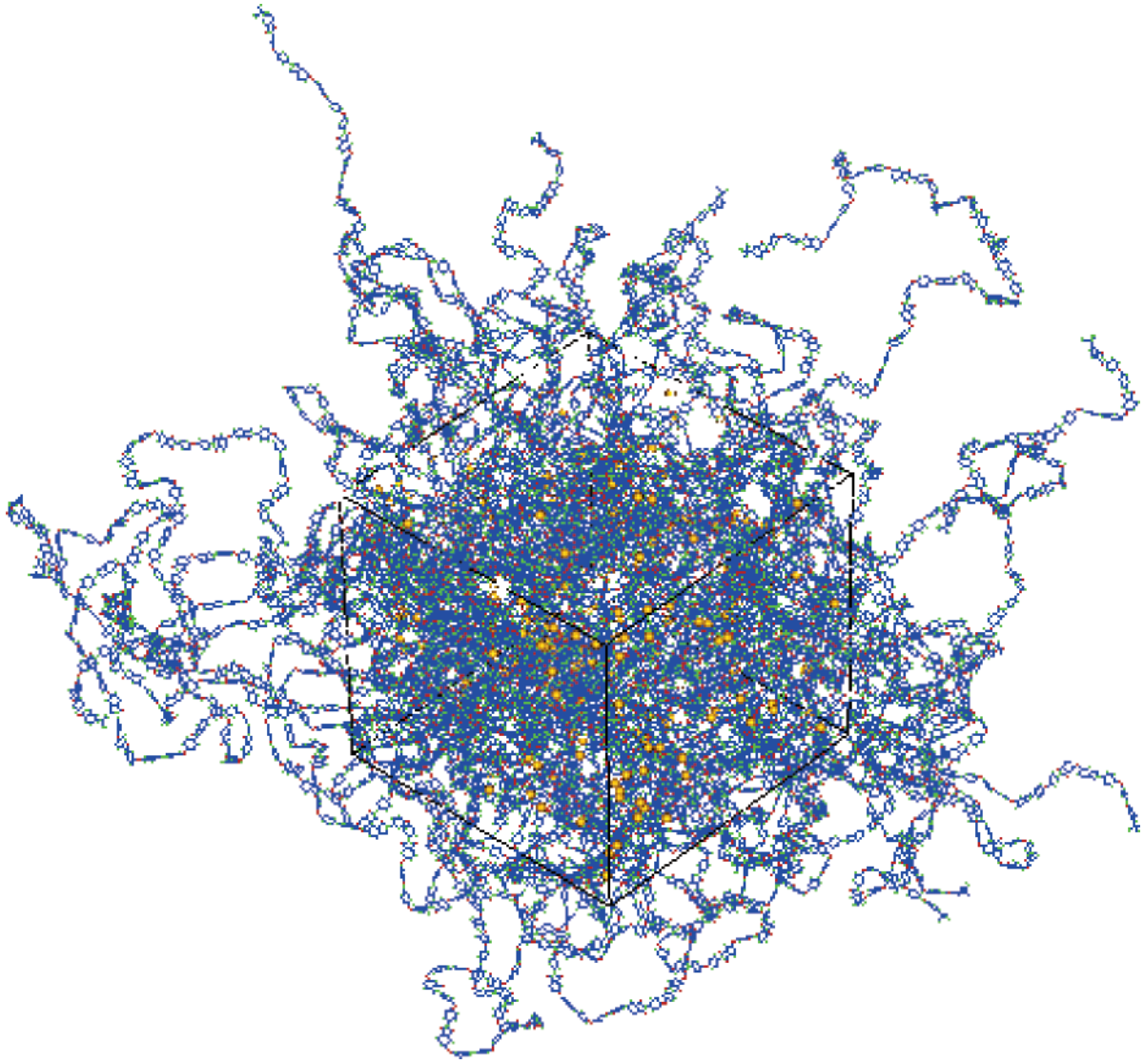

Figure 2. Schematic representation of the 56025-atom model with helium. The polyimide and gas molecules are represented in wire-frame and space-filling models, respectively. Chains are shown in their continuous representation, and the periodic boundary conditions ensure that all the space is filled.

The run production times were 20000 ps for each of the eight 4150-atom systems and 8000 ps for the four 6225-atom and the 56025-atom sizes. A schematic representation of the latter is given in Figure 2.

3. Results and Discussion

3.1. The Polyimide Packing Models. Since the experimental glass-transition temperature for the ODPA−ODA homopolyimide has been measured at ~517 K by differential scanning calorimetry,[19] the models should all be in the glassy state at 300 K. Indeed, polyimide mean-square displacements (MSDs), corresponding to $\langle (r_i(t+t_0) - r_i(t_0))^2 \rangle$ where the angle brackets imply an average over all ODPA−ODA atoms and all possible time origins t_0 of the production runs, are found to be <1 Å^2 for each system under study. Although there is mobility on a local range, there is no overall diffusion of the polyimide chains at 300 K on the MD time scale.

3.1.1. Densities and Energies. As explained earlier, 10 models, i.e., eight 4150-atom, one 6225-atom, and one 56025-atom, were prepared independently. Since the ODPA−ODA homopolyimide has also been investigated experimentally,[19−21] there are a few available data to which these models can be compared. Thermodynamic and structural data are thus given in Table 2 as a function of the system size. The results of the eight 4150-atom models have been averaged in order to compare them with better statistics to the larger models, and the standard deviation of the eight sample means is presented along with the mean values.

Table 2 shows the average relaxed densities $\langle \rho \rangle$, which are all very close to the experimentally determined value of $\rho_{exp} = 1.368$ g cm^{-3}.[19−21] The average pressures of the simulation boxes, $\langle p \rangle$, prove that these densities correspond to atmospheric conditions. $\langle \rho \rangle$ for the 4150-atom systems is almost identical to ρ_{exp} whereas the 6225-atom and 56025-atom systems fall within 0.7% of the experimental value. As has been pointed out before,[18] this is in excellent agreement, which confirms that both the procedure for creating packing models of polyimides in the glassy state and the force field used are adequate for these systems. As far as the 4150-atom systems are concerned, six of these systems fall within less than 1% and two within 2% of the experimental value, which is consistent with the acceptable limit for polyimides as defined by Heuchel, Hofmann, and coworkers.[15,17] The very different sizes are reflected in the average volumes $\langle V \rangle$ of the MD cells, which, to the power

Table 2. Volumetric and Energetic Properties of the Pure Polyimide Systems at 300 K[a]

properties	4150-atom	6625-atom	56025-atom
$\langle r \rangle$	1.367 (0.017)	1.377	1.376
$\langle p \rangle$	0 (3)	2	1
$\langle V \rangle$	47 520 (580)	70 750	637 300
$\langle l \rangle$	36.2 (0.2)	41.4	86.1
$\langle U_{pot}^{inter} \rangle$	−6098 (124)	−6367	−6134
$\langle U_{LJ}^{inter} \rangle$	−5484 (138)	−5669	−5551
$\langle U_{coul}^{inter} \rangle$	−614 (42)	−698	−583
δ	20.65 (0.32)	21.17	20.77

[a] The results for the eight 4150-atom models have been averaged and the numbers in parentheses refer to the standard deviations of the sample means. The maximum standard error corresponds to the estimates obtained from the fluctuations found in one specific sample. The average densities $\langle \rho \rangle$ are given in g cm^{-3} with a maximum standard error of ± 0.001 g cm^{-3}. The average pressures $\langle p \rangle$ are in bars with a maximum standard error of ±2 bar. $\langle V \rangle$ are the average volumes of the MD cells in Å^3 with a maximum standard error of ± 100 Å^3 and $\langle l \rangle = \langle V \rangle^{1/3}$ the "cell length" in Å (all cells are actually slightly triclinic). The average potential intermolecular energies $\langle U_{total}^{inter} \rangle$ as well as their resolution into Lennard-Jones $\langle U_{LJ}^{inter} \rangle$ and Coulombic $\langle U_{coul}^{inter} \rangle$ terms are quoted in kJ mol^{-1} molecule^{-1} with a maximum standard error of ±5 kJ mol^{-1} molecule^{-1}. The Hildebrand solubility parameter, δ, is given in (J cm^{-3})$^{1/2}$ with a standard error of ±0.02 (J cm^{-3})$^{1/2}$.

$^1/_3$, lead to average cell lengths $\langle l \rangle$ of ∼36, ∼41, and ∼86 Å in increasing order. This is based on the assumption that the simulations boxes are quasi-isotropic: indeed, all cell angles oscillate between 89° and 91°. However, despite the large differences in size, the average densities are found to be very similar for all systems under study. There thus does not seem to be any density artifact associated with too-small cell sizes, and the preparation procedure gives reproducible results.[18]

The average intermolecular potential energies, quoted in kJ/mol of molecules, can also be found in Table 2. The average total intermolecular energies $\langle U_{pot}^{inter} \rangle$ have been resolved into their van der Waals $\langle U_{LJ}^{inter} \rangle$ and their electrostatic $\langle U_{coul}^{inter} \rangle$ components. The Hildebrand solubility parameter, δ, is defined as

$$\delta = \sqrt{\frac{\langle U_{pot}^{inter} \rangle}{\langle V \rangle}} \tag{4}$$

As has been noted earlier,[18] the $\langle U_{pot}^{inter} \rangle$ are mostly dominated by the excluded-volume $\langle U_{LJ}^{inter} \rangle$ terms, which amount for 90% of the total intermolecular potential energy, while the remaining is accounted for by the electrostatic $\langle U_{coul}^{inter} \rangle$ interactions. Both the 4150-atom and the 56025-atom energies are very close. On the other hand, the $\langle U_{pot}^{inter} \rangle$ of the 6225-atom system is more stable, suggesting that this system is slightly more cohesive than the others. This is also reflected in the Hildebrand δ parameter. It should be noted that Hildebrand parameters for a polymer can potentially be estimated empirically through the group contribution approach.[64] Although this has been done for a complete series of copolyimides using either the Hoy[65] or the Fedors[66] methods, these empirical parameters (e.g., around 25−28 (J cm^{-3})$^{1/2}$ for the (ODPA−ODA) homopolyimide) were found to be too high to reproduce the experimental solubilities in various solvents.[19] This was linked to the inability of the group contribution approach to take into account the isomeric structures of the rings as well as the lack of parameters for some functional groups and thus could not be used as a validation for our models. Nevertheless, it is interesting that the model δ (Table 2) are lower than the empirical values, which could mean that MD is better suited to extracting these values. In addition, all fall within the normal range of δ = 14−28 (J cm^{-3})$^{1/2}$ reported for polymers.[64]

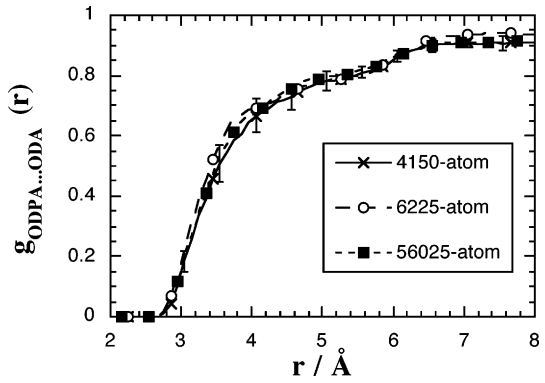

Figure 3. Intermolecular $g_{A\cdots B}(r)$ curves for ODPA with ODA aromatic carbons as a function of system size. The standard deviations refer to the results of the eight different boxes for the 4150-atom size.

3.1.2. Structures. As described earlier,[18,67,68] the indiscriminate intermolecular radial distribution functions for the chains, $g_{inter}(r)$, can be used to check whether the atomistic model systems are really amorphous or whether they exhibit some crystalline characteristics. The $g_{inter}(r)$ functions, calculated over all atoms in a given system, were extracted (results not displayed), and no apparent order was seen. All ODPA−ODA models could thus be considered as amorphous.

The polymer chains configurations can first be characterized by their mean-square radii of gyration, $\langle S^2 \rangle$. For the small systems, the value averaged over the eight $\langle S^2 \rangle$ is 3600 Å^2 with a standard deviation of the sample means of 1110 Å^2, while $\langle S^2 \rangle$ = 3610 Å^2 for the 6225-atom system and $\langle S^2 \rangle$ = 3560 Å^2 for the 56025-atom system. Although these results suggest that the polymer configurations are rather close, they have to be taken with caution, given the very limited statistics on the number of chains (see Table 1). Indeed, the large standard deviation of the sample means is only representative of eight samples of two chains each, which does not provide sufficient statistics to sample the whole population of radii of gyration.

Polyimides are also known to exhibit preferential structural arrangements between dianhydride and/or diamine fragments, with the stacking of planar aromatic rings being fairly common.[18] To compare the intermolecular structure of the different systems under study, better statistics can be obtained from, for example, analyses of specific intermolecular radial distribution functions $g_{A\ldots B}(r)$. Figure 3 shows the $g_{ODPA\ldots ODA}(r)$ which were calculated from the positions of the aromatic carbons belonging to ODPA six-atom ring moieties (type A) and ODA phenyl rings (type B) as a function of system size. These interactions are particularly relevant with regard to the so-called charge-transfer complexes (CTC), which form by electron transfer between electron-rich diamine rings and electron-deficient dianhydride rings.[69] They have been shown to occur in many polyimides by various experimental techniques.[70−75] For example, the ODPA−ODA homopolyimide has a high color index,[18,21] which has

been linked to the formation of CTC.[69] Although the $g_{ODPA...ODA}(r)$ are well-averaged, the intermolecular structure of the different systems is obviously very similar. The same conclusions were found for ODPA···ODPA and ODA···ODA interactions.

As far as conformational properties are concerned, it has been shown that the only real backbone degrees of freedom are the so-called "pivot angles", i.e., rotations around the nitrogen−phenyl bonds of the ODPA−ODA linkages (C−N−C−C torsions) and around the ether linkages of the diamine and ODPA moieties (C−O−C−C torsions).[18] The underlying probability density distributions found in this work (results not displayed) were similar to those described before,[18] i.e., four well-defined peaks located at around ±30° and ±150° for the fairly rigid C−C−N−C angles, while the flexible C−O−C−C ether bridges exhibited much smoother distributions with a small preference for gauche conformations due to H···H repulsions on either side of the rings. In all cases, the 6225-atom and the 56025-atom systems fell within the limits of the average plus or minus the standard deviation of the 4150-atom systems.

3.1.3. Solubilities and Void Spaces. To further validate the quality of our models, solubilities for our full model of He, i.e., using U_{LJ} and U_{coul}, in the ODPA−ODA polyimide were calculated. The solubility, S, is linked to the excess free energy, ΔG, of a gas molecule dissolved in the polymer, the Boltzmann constant k_B, and the temperature T:[26]

$$S = \exp\left(-\frac{\Delta G}{k_B T}\right) \tag{5}$$

In this respect, the (dimensionless) solubility is the ratio between the "volume of gas", V_g, absorbed into a given volume of polymer, V_p, i.e., $S = V_g/V_p$. To be more precise, V_g is the volume the same number of gas molecules (as absorbed into V_p) would occupy if they were in the gas phase at the same conditions of temperature and pressure.

The free energy for the solvation process is usually estimated in atomistic simulations using Widom's test-particle insertion method, in which a gas molecule is inserted at random sites into the matrix and the change in potential energy ΔU associated with the insertion is calculated.[26,62] This process is repeated many times in order to obtain ensemble averages. S is then directly linked to the probability of insertion for the gas molecules into the polymer, p_{ip} :

$$S \approx p_{ip} = \left\langle \exp\left(-\frac{\Delta U}{k_B T}\right)\right\rangle \tag{6}$$

The p_{ip} were thus averaged over all stored configurations of each production run and 1 million trials per configuration.

It is well-known that diffusion and sorption in glassy polymers is traditionally described by the "dual-mode sorption model", in which there are two distinct sorption modes: unspecific dissolution, which follows Henry's law, and trapped molecules in preexisting cavities, which are described by a Langmuir term.[76,77] However, for small and not very soluble penetrants, such as He, sorption follows well Henry's law; i.e., the solubility of dissolved gas is linearly proportional to the pressure, $S = S_c P$, where the "constant" of proportionality, S_c, is called the solubility coefficient. In any case, it has become commonplace to report solubility coefficients in the literature, irrespective of whether Henry's law is obeyed or not. Here we quote solubility coefficients in one of the commonly used forms as $S_c = p_{ip} T_{STP}/(T P_{STP})$, where T_{STP} and P_{STP} are the standard temperature and pressure (STP) and T is the temperature of the experiment. This means that the quantity $S_c P V_p$ represents the volume of gas absorbed in the polymer of volume V_p at the pressure P and temperature T after it has been brought back to STP conditions and assuming it behaved as an ideal gas. Solubility coefficients obtained in this way and expressed in cm^3 (STP) cm^{-3} bar^{-1} are presented in Table 3. They are all of the order of 0.06, which is only slightly higher than the experimentally estimated value S_{eff} of 0.04 cm^3 (STP) cm^{-3} bar^{-1}.[19] The latter were obtained using the relationship between S_{eff} and the experimentally measured effective permeability P_{eff} and diffusion coefficient D_{eff}:[17]

$$S_{eff} = \frac{P_{eff}}{D_{eff}} \tag{7}$$

Table 3. Solubilities and Void Space of the Pure Polyimide Packing Models at 300 K[a]

properties	4150-atom	6225-atom	56025-atom
S_c for He	0.065 (0.007)	0.064	0.059
S_c for Ar−He	0.030 (0.006)	0.029	0.025
S_c for CO_2−He	0.010 (0.005)	0.009	0.007
% PAV (probe radius 0 Å)	34.56 (0.77)	34.17	34.20
% PAV (probe radius 0.4 Å)	13.66 (0.70)	13.56	13.27
% PAV (probe radius 1.1 Å)	1.49 (0.29)	1.45	1.26

[a] The results for the eight 4150-atom models have been averaged and the numbers in parentheses refer to the standard deviations of the sample means. The maximum standard error corresponds to the estimates obtained from the fluctuations found in one specific sample. The solubility coefficients S_c are given in cm^3 (STP) cm^{-3} bar^{-1} with a maximum standard error of ±0.001. They are displayed for the He model considered here as well as for hypothetical "Ar−He" and "CO_2−He" probes differing only in size from the He molecules. The average percentage of probe-accessible volume (% PAV) is shown for nonspecific probes of radii 0, 0.4, and 1.1 Å, respectively, the errors being ±1 on the last figure quoted.

As expected from experimental results,[1,35] the solubility for He into polyimides is much lower than that for other gases, but the values found here are in very good agreement with other polyimides. Indeed, the solubility for He has been reported as being 0.053 and 0.062 cm^3 (STP) cm^{-3} atm^{-1} for PMDA−ODA and PMDA−IPDA.[78]

Since Cuthbert et al. had reported a chain length effect on the solubility of larger penetrants than He in PS,[29] we adopted the same approach than these authors in their more recent paper on glassy PP[30] by considering hypothetical derivatives of helium, namely "argon−helium", Ar−He, and "carbon dioxide−helium", CO_2−He. These particles have the same mass and the same ϵ parameter for the Lennard-Jones potential (eq 1) as helium. However, the penetrant sizes were adjusted by changing σ to 3.405 Å for Ar−He and 4.468 Å for CO_2−He, so as to compare them directly to the results of Cuthbert et al.[30] The resulting solubility coefficients are also presented in Table 3.

Related characteristics to S are the amounts of "void space" available to probes of a given radius. As explained previously,[18] we used a simple Monte Carlo procedure in which probes of a preset radius are

randomly and independently inserted into the MD configurations previously stored. The polymer atoms are represented by hard spheres with standard van der Waals radii, i.e., 1.20 Å for H, 1.50 Å for O, 1.55 Å for N, and 1.70 Å for C.[64,79] Five million trial insertions are attempted for each system, and only those probes that do not overlap with the polyimide atom hard spheres are accepted. The percentage of probe-accessible volume (% PAV) is then equal to the percentage of accepted insertions. The % PAV corresponding to three different probe sizes are presented in Table 3. The zero radius probe represents the total volume "not occupied" by the polymer atoms. The 0.4 Å probe gives the closest values to the free volume fractions (FFV) empirically estimated from the experimental density using the Bondi method,[64,79] i.e., 0.134.[19,21] The 1.1 Å probe corresponds to the "size" of a positronium. All the results are consistent with the grid-based method of Hofmann and co-workers.[53]

It is obvious from Table 3 that average values for the solubilities and % PAV are virtually number independent, even in the case of the larger hypothetical CO_2−He particle. This is in contrast to the results of Cuthbert et al.,[29,30] who linked their system-size-dependent effect in PS to the fact that smaller structures were unable to form cavities of sufficient size to accommodate larger penetrants.[29] Indeed, this bias was confirmed in PP by examining their cavity sizes (see Figure 4 of ref 30) and showing that their smallest structures had narrower sizes distributions. Since their 125mer, 729mer, and 2197mer for PP displayed similar X-ray scattering profiles,[30] it remains unclear whether this bias is due to the generation procedure,[31] the force field used,[30] or more likely the different lengths of the chains and the conditions imposed, e.g., constant densities.

To ensure that the distributions of cavities were not biased in any way in our 10 different ODPA−ODA models, changes in the excess potential energy ΔU associated with the Widom particle insertion process were subaveraged every 1000 insertions for 1 million trials per configuration, still using the full U_{LJ} and U_{coul} potential. The resulting normalized probability distributions of $\Delta U_{1000-ins}/k_BT$ are displayed for He, Ar−He, and CO_2−He particles in parts a, b, and c of Figure 4, respectively. Standard deviations calculated from the eight different simulations of the 4150-atom size are indicated in order to characterize the dispersion of the results. Figure 4 shows that there is a large amount of heterogeneity in the void distributions, which is reflected both in the actual distributions of $\Delta U_{1000-ins}/k_BT$ and in the standard deviations displayed. This is especially obvious for the large cavities corresponding to the smaller $\Delta U_{1000-ins}$. However, if one considers the normal differences that can be expected from the standard deviations of the 4150-atom size, there is no real bias in the cavity size distributions of the larger 6225-atom and 56025-atom systems. It is interesting to note that when the diameter of the inserted particles is bigger, i.e., in increasing order He < Ar−He < CO_2−He, the distributions of excess chemical potentials get progressively wider and skewed to the right, indicating that there are fewer holes of the size that can easily accommodate particles of larger sizes. On the other hand, the distributions for particles as small as He are quite symmetric in terms of large and small cavities, which suggests that this gas can potentially access most of the void space available without too much disruption

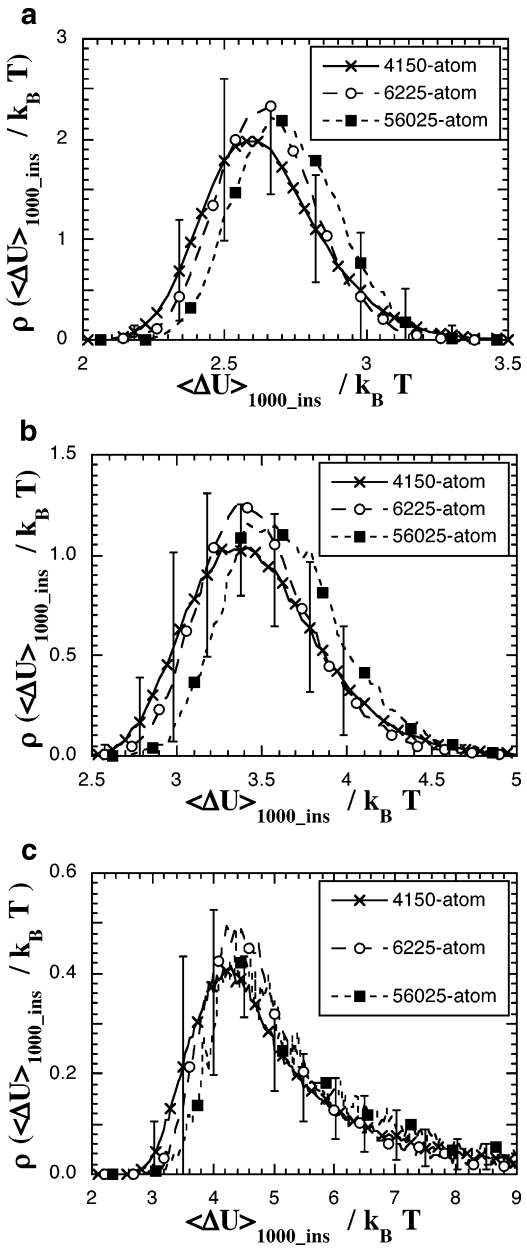

Figure 4. Normalized probability distributions of the changes in excess potential energy associated with the Widom particle insertion technique and subaveraged every 1000 insertions, $\Delta U_{1000-ins}$, accumulated for 1 million trials per configuration. The inserted particles are (a) He, (b) the hypothetical "Ar−He", and (c) the hypothetical "CO_2−He" particles defined as in the text. The standard deviations refer to the results of the eight different boxes for the 4150-atom size.

of the glassy polyimide matrix. However, regardless of the penetrant diameter, all solubility results are number independent within errors. This is corroborated by an additional series of % PAV analyses as a function of probe size in our polyimide models, including hard spheres of radius larger than He (results not shown). The use of only one chain length for the ODPA−ODA polyimide as well as constant-pressure rather than constant-density conditions thus avoids the cavity size bias reported by Cuthbert et al.[29,30]

3.2. Simulation Size Effect on Diffusion. As mentioned in section 2, helium molecules were inserted into each of the 10 polyimide matrices (Table 1), and the resulting systems were run using the less costly WCA form of the "nonbonded" potential (eq 3), U_{WCA},

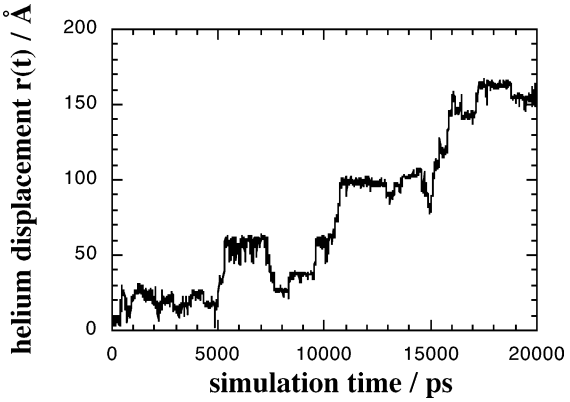

Figure 5. Typical displacement of a helium atom in one of the 4150-atom systems as a function of simulation time.

instead of the full combination of Lennard-Jones and electrostatic potentials (eqs 1 and 2). Although this can be justified taking into account that the overall structure of the glassy polyimide matrices is hardly modified and that helium molecules are uncharged, it is obvious that diffusion will not be directly comparable to the "real" experimental systems. On the other hand, this allowed us to simulate for far longer times (Table 1), i.e., up to 20 ns for all eight 4150-atom systems and up to 8 ns for the larger simulation boxes, and thus to assess, with good statistics, the number dependence of diffusivity. In addition, as mentioned earlier, four different simulations for the 6225-atom pure matrix were run from that specific configuration, each starting with independently inserted positions for the gas molecules.

3.2.1. Diffusion Mechanisms. The trajectories of individual helium molecules were first examined to characterize the mechanisms underlying their mobility in the matrix. A typical path over 20 ns of production time is shown in Figure 5. As has been seen before for polyimides,[11−14,49] the individual displacements are obtained by a combination of oscillations within available free volumes and jumping events. These patterns have been shown to be characteristic of a diffusion which proceeds by hopping between different voids, made possible by the temporary opening of channels within the polymer matrix.[26,27] Although the glassy ODPA−ODA chains are fairly rigid, they do undergo natural fluctuations on the scale of, at the most, 1 or 2 Å and can form a passage for the helium molecules. The time scale for the jumps displayed in Figure 5 are typically of the order of 50−100 ps. The relationship between the matrix-limited fluctuations and helium transport has been clearly pointed out by TSA simulations of glassy polycarbonate.[80] Since such a mechanism is activated by the local motions of the chains, it is fundamentally different from the aforementioned percolating networks of Weber et al.[28] or Boshoff et al.[32]

Although not liquidlike, helium diffusion in glassy polymers generally resembles closely what is seen in the rubbery state with large jumps and quite effective diffusivity because of its high intrinsic mobility. Even if the individual molecules can oscillate within the same site for typically several hundred picoseconds and occasionally get temporarily "trapped" in a dead end, they always reach a position that allows them to take another path (see Figure 5). A similar type of behavior has been found for hydrogen in polyimides.[11−14] On the other hand, slower penetrants such as water[49] or oxygens[13,14] will have a tendency to undergo much shorter jumps or even to jump back and forth between different voids, thus leading to very limited diffusion. It has been pointed out in a penetrant size comparison that, when small molecules are studied, the steplike jumps are much less pronounced, and the positional fluctuations at a given site are larger, thus leading to a certain "blur" in the trajectories.[26,27] This is exactly what is found in the present work, with a large variety of patterns for the helium molecules, whether they belong to a 4150-atom, 6225-atom, or 56025-atom systems. No specific system size behavior could be detected from the individual trajectories. Even if some gas molecules in the smaller sizes eventually visit the periodic images of the initial polyimide box, the local motion of the matrix and the many possible paths for helium transport prevent a periodicity artifact in the trajectories.

3.2.2. Einstein Diffusion. Although there are several methods available to evaluate diffusion coefficients from MD simulations,[30] the most common way involves the calculation of mean-square displacements, MSDs = $\langle (r_i(t+t_0) - r_i(t_0))^2 \rangle$, averaged over all penetrant molecules and all possible time origins of the production runs, t_0. The MSDs can then be used to evaluate the corresponding diffusion coefficients using Einstein's equation:

$$D = \lim_{t\to\infty} \frac{1}{6t} \langle (r_i(t+t_0) - r_i(t_0))^2 \rangle \tag{8}$$

However, the derivation of the Einstein equation assumes that the gas molecules follow a random walk. In dense polymers, where penetrant motion is strongly restricted by the immediate environment, Einstein's equation is only really valid within the framework of a long-time Fickian diffusive limit, i.e., when the MSDs are proportional to t. In the intervening time, with the exception of a short-time ballistic regime at the very start, the MSD curves are usually found to be proportional to t^n with $n < 1$, which characterizes the anomalous diffusion regime.[26,27] The turnover or crossover time defines that region when diffusion goes from being anomalous to Fickian and is best identified on log−log plots, when the slope between log(MSDs) and log(t) tends to one.[26]

The log−log plot corresponding to our He MSDs is presented for the three sizes under study in Figure 6a. Also shown for comparison is a straight line of slope 1. It is clear that the crossover region for all these systems is around 1000 ps. Indeed, from 1000 ps, the slopes are at least 0.91, which are within the limits of 1.0 ± 0.1 defined by Cuthbert and Wagner et al.[30,32] for the characterization of Fickian diffusion. The problem of actually defining a crossover time and distance is illustrated in Figure 6b for the average MSDs of the smallest 4150-atom size. The crossover between the two regimes is very gradual, and it is not particularly obvious to identify. We chose a similar approach to Boshoff et al.[32] in their work on helium motion in frozen polypropylene matrices, where they first fitted the anomalous regime to MSDs $\propto t^{0.5}$ and the Fickian regime to MSDs $\propto t$ and then defined the crossover time and distances as the intersection between the two fits. We did not manage to fit our MSDs to $t^{0.5}$ (which would be representative of dynamics consistent with the center-of-mass diffusion of a reptating chain, i.e. with one-dimensional tubelike motion[32]), but they did fit well to the form t^n with $n < 1$ over the first 500 ps of the

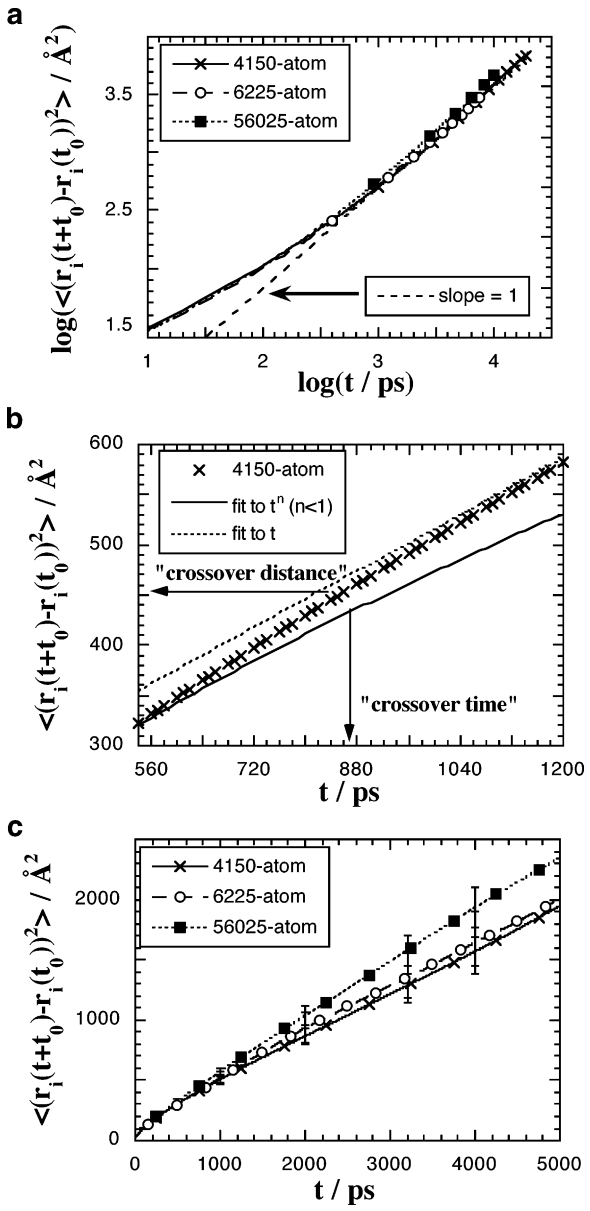

Figure 6. Helium MSDs vs time for the three system sizes under study: (a) The log−log plot along with a dashed straight line of slope 1. The diffusion goes from the anomalous to the Fickian regime when the slopes of the other curves reach the value of 1. (b) The crossover region for the averaged MSDs of the 4150-atom size along with a fit to the form t^n with $n < 1$ for the anomalous regime and another fit to the form t in the Fickian regime. The crossover time and distance are defined to be the average point during the gradual change of regime. (c) Comparison of the actual MSDs, averaged over all production time origins separated by 10 ps. For an explanation of the error bars, see the text.

anomalous regime. The powers found were 0.63 for the 4150-atom, 0.65 for the 6225-atom, and 0.68 for the 56025-atom sizes. The corresponding fits to the Fickian regimes of the MSDs were also obtained (MSDs $\propto t$). As can be shown from Figure 5b, both fits did not cross, but the change from the anomalous to the Fickian regime is very noticeable over a graphically defined analysis interval. In this work, the crossover times and distances were empirically attributed to the average point during the gradual change of regime, and they are given in Table 4. Within the obvious uncertainties linked to the graphical determination of the crossover time, no significant differences can be noticed in Table 4. In all cases, the crossover distance occurs at smaller values than the box length (see Table 2), which is once again in disagreement with the results of Cuthbert et al. for helium in glassy PP.[30] However, the same authors reported that the Ar−He and CO_2−He penetrants did reach the diffusive regime before traveling a box length in their simulations,[30] thus suggesting that the difference might more be due to the various potentials used rather than to the box length effect. In contrast, Weber and Paul gave a critical box size for their percolating static polymer systems, below which the crossover seemed to occur when MSDs corresponded to the box length.[28] Above that critical box size, the diffusion coefficient and the turnover point became independent of box size.[28] Boshoff et al. found a similar size dependence for He in frozen glassy PP,[32] which was much more pronounced than He in mobile glassy PP.[30] The differences between the results for the frozen and mobile matrices were attributed to changes of the penetrant diffusion mechanism from an activated diffusion process to a kinetic motion hindered by tortuosity.[32] While the critical box size was very large for the coarse-grained models of Weber et al.,[28] it was closer to our systems in the work of Boshoff et al.,[32] i.e., >40 Å, which is larger than our 4150-atom simulations and roughly the size of the 6225-atom model. In the present work, our polyimide chains are mobile, albeit in a fairly limited way, and we do not see such a critical limit.

Table 4. Helium Diffusion Crossover Times and Distances from the Anomalous to the Fickian Regime As Defined Graphically According to the Procedure Described in Figure 5b

properties	4150-atom	6225-atom	56025-atom
time interval for the crossover/ps	540−1200	500−1500	550−1200
crossover time/ps	870	1000	875
crossover distance/Å	21.3	22.7	22.6

All three MSDs vs time curves for the anomalous and Fickian diffusion regimes are shown in Figure 6c. The error bars displayed in Figure 6c are the standard errors calculated from the number of gas molecules and the number of uncorrelated time origins in a given system and multiplied by 2.58 in order to give the 99% interval span that can be expected from the normal law. In addition, the smallest systems results have been averaged together for the 4150-atom size as well as the four independent gas-starting-positions runs for the 6225-atom size, and this has also been taken into account in the error bars. Figure 6c proves that these three system sizes can basically be considered as equivalent.

The actual diffusion coefficients obtained from the Fickian regime of the MSDs curves using eq 8 are $D_{4150-\mathrm{atom}} = 6.0 \times 10^{-6}$ cm^2 s^{-1}, $D_{6225-\mathrm{atom}} = 6.7 \times 10^{-6}$ cm^2 s^{-1}, and $D_{56025-\mathrm{atom}} = 7.5 \times 10^{-6}$ cm^2 s^{-1}. The error bars on the MSDs can also be used to give limiting values, with an overall lower bound of $D = 4.8 \times 10^{-6}$ cm^2 s^{-1} and an upper bound of $D = 8.2 \times 10^{-6}$ cm^2 s^{-1} for the diffusion coefficient of He in our ODPA−ODA polyimide matrices. Although these bounds roughly differ by a factor 1.7, it is not enough to explain the discrepancy between simulation and experiment ($D_{\mathrm{simulation}} = 1.0 \times 10^{-5}$ cm^2 s^{-1} using U_{LJ} and U_{coul} for nonbonded interactions while $D_{\mathrm{experiment}} = 5.0 \times 10^{-7}$ cm^2 s^{-1}) for that specific polyimide which was the initiator of this work.[19] The apparent trend, if it were statistically significant, is also toward higher diffusion coefficients for larger systems, the contrary of what

would be expected from the "percolating channels" hypothesis. Reasons others than number dependence will thus have to be sought to explain this difference. However, it is interesting to note that, despite using U_{WCA} instead of U_{LJ} and U_{coul}, the order of magnitude of the diffusion coefficients found here is reasonable for helium in glassy polyimides. Indeed, experimental results for a variety of polyimides report values in the range $\sim(1-8) \times 10^{-6}$ cm^2 s^{-1},[78] or more generally from 10^{-5} to 10^{-7} cm^2 s^{-1}.[19]

3.2.3. Distributions of Penetrant Displacement Components. To further ensure that our gas mobility results are number independent, we have determined the underlying probability density distribution of displacement vector components, $\rho(\alpha(t+t_0) - \alpha(t_0))$, where t is the time interval, t_0 is the time origin, and α represents x, y, or z. These have already been presented for the case of water diffusion in short polyimides.[63] In that specific case, the Fickian regime could not be reached because of the low mobility of the water molecules. However, diffusion in the anomalous regime could be well characterized[63] by these distributions.

To have better statistics for the $\rho(\alpha(t+t_0) - \alpha(t_0))$, averages were taken over all possible time origins for the production simulation, only the absolute values of the components were used, and displacements along the x, y, and z axes were averaged together for all penetrant atoms. As before, the 4150-atom results were averaged over the eight different systems and those for the 6225-atom size over the four systems with different initial He positions. The displacement component distribution for a $t = 100$ ps time interval is given just for the 56025-atom system in Figure 7a. Distributions for the other system sizes at this and other time intervals were the same, within errors, so no number-dependent effects are apparent.

The general shape of the curves is similar to that found for water diffusion in polyimides.[63] As before,[19,63] these distributions in the anomalous regime could not be fitted by the single Gaussian curve expected from Fickian diffusion:

$$\rho(\alpha(t+t_0) - \alpha(t_0)) = \sqrt{\frac{3}{2\pi\langle r^2\rangle}} \exp\left(-\frac{3}{2\langle r^2\rangle}\alpha^2\right) \quad (9)$$

with $\langle r^2\rangle = \langle x^2\rangle + \langle y^2\rangle + \langle z^2\rangle$. However, the anomalous regime distributions do fit surprisingly well to a weighted combination of two Gaussian curves

$$\rho(\alpha(t+t_0) - \alpha(t_0)) = \omega(t)\left(\sqrt{\frac{3}{2\pi\langle r_1^2\rangle}} \exp\left(-\frac{3}{2\langle r_1^2\rangle}\alpha^2\right)\right) + (1-\omega(t))\left(\sqrt{\frac{3}{2\pi\langle r_2^2\rangle}} \exp\left(-\frac{3}{2\langle r_2^2\rangle}\alpha^2\right)\right) \quad (10)$$

Previously, this was attributed to two distinct types of time-dependent behavior. The first one, with average displacement $\langle r_1^2\rangle$, was referred to as type "1" and was interpreted as being related to those molecules that remain in, or return to, the very near vicinity of their position at the time origin, i.e., molecules which can be considered as being "trapped". The second one, with average displacement $\langle r_2^2\rangle$, was referred to as type "2" and was interpreted as being related to those molecules which escape from their initial environments, i.e., which will eventually contribute to the limiting long-time diffusion coefficient. The weighting factor, $\omega(t)$, represents the respective proportions of both types of populations for a given time interval, t. Although these distributions are for components (and not the modulus) of the vector displacement, this simple interpretation does agree very well with visual analyses of the individual trajectories and the van Hove correlation functions (see later).

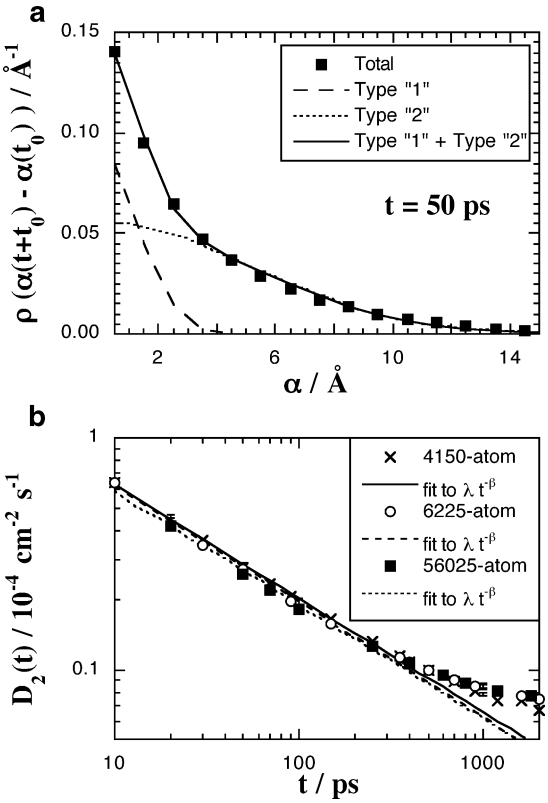

Figure 7. (a) Probability density distributions for the components of the displacement vector for the helium atoms at the $t = 50$ ps time interval in the 56025-atom system. The actual curve is shown in black squares. The dashed lines represent the two weighted Gaussians fitted to the actual data (eq 10), i.e., populations of types "1" and "2", respectively. The weighting factor $\omega = 0.29$, $\langle r_1^2\rangle = 4.85$ Å^2, and $\langle r_2^2\rangle = 77.87$ Å^2. The plain line is the sum of both Gaussians for types "1" and "2". (b) Time evolution of the helium diffusion coefficient for type "2", $D_2(t)$, as defined in eq 11. The actual simulation points are the crosses for the 4150-atom size, the circles for the 6225-atom size, and the squares for the 56025-atom size. The lines are fits to the algebraic form $D_2(t) = \lambda t^{-\beta}$ for the three sizes under study in increasing order. The error bars on $D_2(t)$ are indicated for $t = 20$, 50, 100, 500, and 1000 ps.

For the smallest time interval considered in this work, i.e., 10 ps, ω is found to be $\sim$0.34 for the 4150-atom, $\sim$0.36 for the 6225-atom, and $\sim$0.37 for the 56025-atom size. This is significantly lower than the ω for water in polyimides ($\sim$0.6)[63] because of the much higher mobility of helium. The weighting factor decreases rapidly as the time interval increases (e.g., $\omega \sim 0.25$ in the $t = 100$ ps distribution shown in Figure 7a) and drops to 0.10 after a time interval of $\sim$1000 ps. This confirms the crossover region from the anomalous to the Fickian regime whereafter the displacement vector component distributions can then be fitted satisfactorily to the single Gaussian expression of eq 9.

An advantage of this method is that it characterizes diffusion at both short and long distances. In the anomalous regime, $\langle r_1^2\rangle$ increases slower and slower as

a function of time and eventually tends toward a plateau value between 10 and 14 Å^2 around 1000 ps. It is not easy to establish the plateau value with more precision due to the poor statistics ($\omega < 0.1$) at longer times. This is consistent with those gas atoms which oscillate within cavities and take some time to fully explore them. On the other hand, the $\langle r_2^2 \rangle$ of the fitted Gaussian are much larger and can be used to define "time-dependent" diffusion coefficients, $D_2(t)$:

$$D_2(t) = \langle r_2^2 \rangle / 6t \tag{11}$$

The $D_2(t)$ coefficients are displayed on a logarithmic scale in Figure 7b for all three system sizes. The decrease of $D_2(t)$ in the anomalous regime (<1000 ps) can be fitted to the algebraic form $D_2(t) = \lambda t^{-\beta}$, with $\lambda = 1.93$, 1.96, 1.84 and $\beta = 0.49$, 0.50, 0.49 for the 4150-, 6225-, and 56025-atom sizes, respectively. These fits are indicated by the straight lines in Figure 7b, while the actual $D_2(t)$ are shown as symbols only. The algebraic form fits well the anomalous regime, but it cannot be valid in the Fickian regime as it does not lead to a nonzero asymptote at long times. However, in parallel to the decrease of the weighting factor, this is an alternative way to identify the crossover region from the anomalous to the Fickian regime. The Einstein diffusion coefficients, identified from the long-time behavior of the displacement distributions, are found to be $D_{4150-\mathrm{atom}} = 6.3 \times 10^{-6}$ cm^2 s^{-1}, $D_{6225-\mathrm{atom}} = 7.2 \times 10^{-6}$ cm^2 s^{-1}, and $D_{56025-\mathrm{atom}} = 8.0 \times 10^{-6}$ cm^2 s^{-1}, i.e., also in agreement with those obtained from the MSDs vs time curves. This confirms the conclusions drawn before.

3.2.4. Distributions of Penetrant Displacement Distances. The previous analyses were completed by considering the self-part of the van Hove correlation function, as has been done in other studies.[30,32] The van Hove self-correlation function $G_s(r,t)$ gives the probability density that a penetrant moves a distance, r, over a given time interval, t. The $G_s(r,t)$ distributions for the 56025-atom system at different time intervals are given in Figure 8a, along with the corresponding fits to the limiting form in the Fickian regime which are defined[81] as

$$G_s(r,t) = (4\pi Dt)^{-3/2} \exp(-r^2/4Dt) \tag{12a}$$

or alternatively, if the diffusion coefficient D is replaced by $\langle r^2 \rangle / 6t$, by

$$G_s(r,t) = (2\pi \langle r^2 \rangle / 3)^{-3/2} \exp(-3r^2/2\langle r^2 \rangle) \tag{12b}$$

As could be expected, the fits of the actual $G_s(r,t)$ to eq 12 in the anomalous regime, i.e., up to 1000 ps, are poor. On the other hand, the data at longer times become consistent with the limiting form expected, and the fits can be used to evaluate D for the various sizes under study. For a time interval of $t = 4000$ ps, the average values are found to be $D_{4150-\mathrm{atom}} = 5.9 \times 10^{-6}$ cm^2 s^{-1}, $D_{6225-\mathrm{atom}} = 6.8 \times 10^{-6}$ cm^2 s^{-1}, and $D_{56025-\mathrm{atom}} = 7.6 \times 10^{-6}$ cm^2 s^{-1}, i.e., necessarily close to those obtained using the other analyses.

In Figure 8b, the van Hove functions at $t = 50$ ps are shown for all three system sizes under study. As before, there is no obvious number dependence in the results. It is interesting to note, however, that the van Hove functions in the anomalous regime exhibit a shoulder or even a double peak form. This appears to be consistent with the notion of two populations identified in the penetrant displacement component distributions. In a similar vein to eq 10, a fit of the data to the following weighted two-population form was attempted:

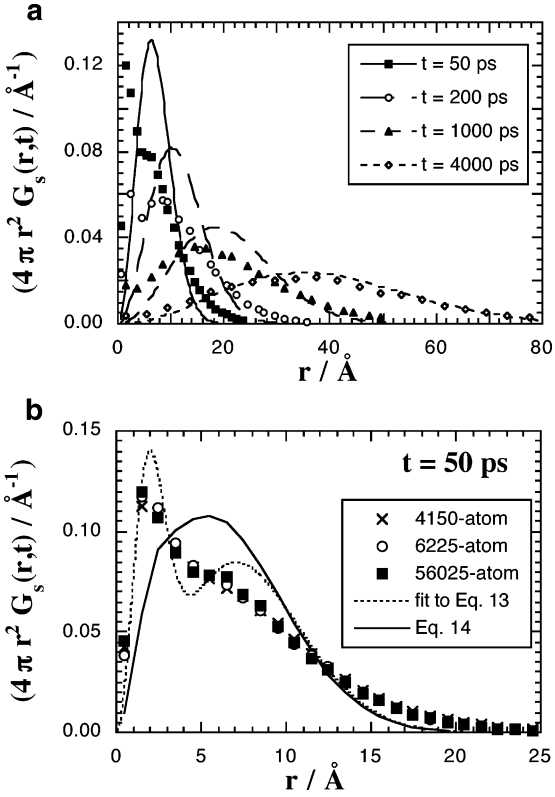

Figure 8. (a) Van Hove self-correlation functions for He in the 56025-atom system at different time-intervals, i.e., 50, 200, 1000, and 4000 ps. The actual data are shown in symbols only. The associated lines are the corresponding fits to the limiting form of the van Hove self-correlation function given in eq 12. (b) The van Hove self-correlation function at the $t = 50$ ps time interval. The actual simulation points are the crosses for the 4150-atom size, the circles for the 6225-atom size, and the squares for the 56025-atom size. The dashed line is a tentative fit to the weighted form of eq 13 for the 56025-atom system, and the plain line is obtained from eq 14.

$$G_s(r,t) = \omega(t)((2\pi\langle r_1^2 \rangle/3)^{-3/2} \exp(-3r^2/2\langle r_1^2 \rangle)) + (1 - \omega(t))((2\pi\langle r_2^2 \rangle/3)^{-3/2} \exp(-3r^2/2\langle r_2^2 \rangle)) \tag{13}$$

with $\langle r_1^2 \rangle$ and $\langle r_2^2 \rangle$ again being the average displacements for type "1" and "2", respectively, at a time interval t. From Figure 8b, it is clear that the best fit to eq 13 is much less successful at describing the data for $G_s(r,t)$ than eq 10 is of matching the displacement vector component distributions. Adding further terms to eq 13 gives progressively better fits, as has been found before,[32] but it is difficult to link it to a physical basis. To clarify why there was such a difference, the double-Gaussian fits (eq 10) to the vector displacement component distributions were used to estimate the corresponding vector displacement magnitude distributions, $\rho(|\mathbf{r}|)$ ($= 4\pi r^2 G_s(r,t)$), assuming that the probability of a given displacement vector, $\rho(\mathbf{r})$, is simply proportional to $\rho(x)\rho(y)\rho(z)$, i.e.

$$\rho(|\mathbf{r}|) \propto \int_{\phi=0}^{\phi=\pi} \int_{\theta=0}^{\theta=2\pi} \rho(x)\, \rho(y)\, \rho(z)\, r^2 \sin\phi \, \mathrm{d}\phi \, \mathrm{d}\theta \tag{14}$$

where the displacement vector $\mathbf{r} = (x, y, z)$. The curve obtained by numerically integrating eq 14 in the case

of $t = 50$ ps for the 56025-atom size is also displayed in Figure 8b. It manifestly fails to predict the actual form of the $4\pi r^2$-weighted van Hove function which means that $\rho(\mathbf{r}) \neq \rho(x)\rho(y)\rho(z)$. In other words, the components of the displacement vector cannot be considered as being independent in the anomalous diffusion regime. The polymer matrix imposes a correlation in the motion of the gas atoms and restricts the penetrant motion,[26] which is particularly important for short displacement vectors, i.e., at short times. For longer times (larger displacement vectors) the correlation in the motion is, of course, still there, but proportionally it becomes less and less significant and hence the Fickian regime is progressively attained.

4. Conclusions

The system size effect observed by Cuthbert et al.[29,30] for solubility in glassy polymer matrices seems to be directly related to the morphology of their packing models, where a bias in their cavity size distributions was identified. Whether this is a genuine chain length effect is difficult to say as the role played by the imposition of a constant density for chains of different lengths is hard to assess. However, in the present work, the generation procedure for our polyimide chains, which uses PMC−MD single-chain sampling[49] followed by a thorough relaxation procedure,[18] leads to a series of glassy ODPA−ODA models which are all slightly different but remain consistent with each other, despite the different number of chains in the system. Indeed, this is clearly shown by analyzing the average densities, intermolecular energies, Hildebrand parameters, mean-square radii of gyration, radial distribution functions, conformational distributions, amount of probe-available void space, and solubilities for the 4150-atom, 6225-atom, and 56025-atom pure matrices. In addition, standard deviations for the various properties under study could be obtained from the eight independent 4150-atom systems, thus assessing the dispersion of the results. The distributions of excess chemical potentials using different probe sizes are especially relevant with respect to refs 29 and 30 since they show that the use of only one chain length for the ODPA−ODA polyimide, the aforementionned generation procedure for the packing models, and constant-pressure conditions does not lead to any cavity size bias.

Despite the use of the less costly WCA instead of the full Lennard-Jones and Coulombic forms for the "non-bonded" potentials, the diffusion mechanism of helium remains characteristic of large jumps between different voids in the glassy matrix, which are directly activated by the local motions of the chains. The four different analyses concerning diffusion, i.e., consideration of the individual trajectories, mean-square displacements, distributions of penetrant displacements components, and van Hove correlation functions, tend to confirm some conclusions of Cuthbert et al. for glassy polypropylene.[30] Indeed, if these authors did report a chain length effect on solubility, they also showed that simulation size did not have a significant effect on the diffusive motion of their penetrants (with the exception of a slight effect for helium).[30] In this work, we show that diffusion, whether it is in the anomalous or in the Fickian regime, is, within errors, number independent. Consequently, it can be pointed out that permeability, which is obtained by the product of the diffusion coefficient and the solubility, is itself number independent in these systems.

As mentioned above, the estimation of a factor of 1.7 between the lowest and highest limit for the diffusion coefficient is not sufficient to explain the discrepancies between simulated and experimental diffusion coefficients[19] that initiated this work. Other reasons, such as the influence of the combination rules for the polyimide−gas cross-term parameters[82] and the surface effect,[83] are currently being investigated.

Acknowledgment. The IDRIS (Orsay, France) and the CINES (Montpellier, France) supercomputing centers are acknowledged for the provision of computer time as well as local resources at the University of Savoie (COMPAQ DS20E). The Rhône-Alpes region is thanked for funds dedicated to computer hardware and A. Douanne for helping with the hybrid PMC−MD sampling of the polyimide.

References and Notes

(1) *Polyimides: Fundamentals and Applications*; Marcel Dekker: New York, 1996.
(2) Ohya, H.; Kudryavtsev, V. V.; Semenova, S. I. *Polyimide Membranes−Applications, Fabrication and Properties*; Kodansha Ltd. and Gordon and Breach Science Publishers S.A.: Tokyo and Amsterdam, 1996.
(3) *Polymeric Gas Separation Membranes*; Paul, D. R., Yampolskii, Y. P., Eds.; CRC Press: Boca Raton, FL, 1994.
(4) Pandey, P.; Chauhan, R. S. *Prog. Polym. Sci.* **2001**, *26*, 853.
(5) McHattie, J. S.; Koros, W. J.; Paul, D. R. *Polymer* **1991**, *32*, 2618.
(6) Chen, K. M.; Wang, T. H.; King, J. S. *J. Appl. Polym. Sci.* **1993**, *48*, 291.
(7) Allen, M. P.; Tildesley, D. J. *Computer Simulation of Liquids*; Clarendon Press: Oxford, England, 1987.
(8) Smit, E.; Mulder, M. H. V.; Smolders, C. A.; Karrenbeld, H.; Van Eerden, J.; Feil, D. *J. Membr. Sci.* **1992**, *73*, 247.
(9) Zhang, R.; Mattice, W. L. *J. Membr. Sci.* **1995**, *108*, 15.
(10) Ayala, D.; Lozano, A. E.; De Abajo, J.; García-Perez, C.; De la Campa, J. G.; Peinemann, K.-V.; Freeman, B. D.; Prabhakar, R. *J. Membr. Sci.* **2003**, *215*, 61.
(11) Hofmann, D.; Ulbrich, J.; Fritsch, D.; Paul, D. *Polymer* **1996**, *37*, 4773.
(12) Hofmann, D.; Fritz, L.; Ulbrich, J.; Paul, D. *Polymer* **1997**, *38*, 6145.
(13) Hofmann, D.; Fritz, L.; Ulbrich, J.; Paul, D. *Comput. Theor. Polym. Sci.* **2000**, *10*, 419.
(14) Hofmann, D.; Fritz, L.; Ulbrich, J.; Schepers, C.; Böhning, M. *Macromol. Theory Simul.* **2000**, *9*, 293.
(15) Heuchel, M.; Hofmann, D. *Desalination* **2002**, *144*, 67.
(16) Fritsch, D.; Peinemann, K. V. *J. Membr. Sci.* **1995**, *99*, 29.
(17) Heuchel, M.; Hofmann, D.; Pullumbi, P. *Macromolecules* **2004**, *37*, 201.
(18) Pinel, E.; Brown, D.; Bas, C.; Mercier, R.; Albérola, N. D.; Neyertz, S. *Macromolecules* **2002**, *35*, 10198.
(19) Pinel, E. Ph.D. Thesis, University of Savoie, Le Bourget-du-Lac, France, 2001.
(20) Pinel, E.; Bas, C.; Neyertz, S.; Albérola, N. D.; Petiaud, R.; Mercier, R. *Polymer* **2002**, *43*, 1983.
(21) Pinel, E.; Barthe, M.-F.; De Baerdemaeker, J.; Mercier, R.; Neyertz, S.; Albérola, N. D.; Bas, C. *J. Polym. Sci., Part B: Polym. Phys.* **2003**, *41*, 2998.
(22) Fisher, J.; Lago, S. *J. Chem. Phys.* **1983**, *78*, 5750.
(23) Cheung, P. S. Y.; Powles, J. G. *Mol. Phys.* **1975**, *30*, 921.
(24) Müller-Plathe, F.; Rogers, S. C.; Van Gunsteren, W. F. *Macromolecules* **1992**, *25*, 6722.
(25) Müller-Plathe, F.; Rogers, S. C.; Van Gunsteren, W. F. *J. Chem. Phys.* **1993**, *98*, 9895.
(26) Müller-Plathe, F. *Acta Polym.* **1994**, *45*, 259.
(27) Gusev, A. A.; Müller-Plathe, F.; Van Gunsteren, W. F.; Suter, U. W. *Adv. Polym. Sci.* **1994**, *116*, 207.
(28) Weber, H.; Paul, W. *Phys. Rev. E* **1996**, *54*, 3999.
(29) Cuthbert, T. R.; Wagner, N. J.; Paulaitis, M. E. *Macromolecules* **1997**, *30*, 3058.
(30) Cuthbert, T. R.; Wagner, N. J.; Paulaitis, M. E.; Murgia, G.; D'Aguanno, B. *Macromolecules* **1999**, *32*, 5017.
(31) Kotelyanskii, M. J.; Wagner, N. J.; Paulaitis, M. E. *Macromolecules* **1996**, *29*, 8497.

(32) Boshoff, J. H. D.; Lobo, R. F.; Wagner, N. J. *Macromolecules* **2001**, *34*, 6107.
(33) Yamamoto, H.; Mi, Y.; Stern, S. A.; St-Clair, A. K. *J. Polym. Sci., Part B: Polym. Phys.* **1990**, *28*, 2291.
(34) Jia, L.; Xu, J. *Polym. J.* **1991**, *23*, 417.
(35) Stern, S. A. *J. Membr. Sci.* **1994**, *94*, 1.
(36) Li, Y.; Ding, M.; Xu, J. *Macromol. Chem. Phys.* **1997**, *198*, 2769.
(37) Brown, D., *gmq* user manual, 2001. Available at http://www.univ-savoie.fr/labos/lmops/brown/gmq.html.
(38) Clark, M.; Cramer III, R. D.; Van Opdenbosch, N. *J. Comput. Chem.* **1989**, *10*, 982.
(39) Hammonds, K. D.; Ryckaert, J.-P. *Comput. Phys. Commun.* **1991**, *62*, 336.
(40) Ewald, P. P. *Ann. Phys.* **1921**, *64*, 253.
(41) Smith, W. *Comput. Phys. Commun.* **1992**, *67*, 392.
(42) Lee, J. F.; Sears, F. W.; Turcotte, D. L. *Statistical Thermodynamics,* 2nd ed.; Addison-Wesley: Reading, MA, 1973.
(43) Brown, D.; Clarke, J. H. R.; Okuda, M.; Yamazaki, T. *J. Chem. Phys.* **1994**, *100*, 1684.
(44) Brown, D.; Clarke, J. H. R.; Okuda, M.; Yamazaki, T. *J. Chem. Phys.* **1994**, *100*, 6011.
(45) Brown, D.; Clarke, J. H. R.; Okuda, M.; Yamazaki, T. *J. Chem. Phys.* **1996**, *104*, 2078.
(46) Neyertz, S.; Brown, D. *J. Chem. Phys.* **1995**, *102*, 9725.
(47) Neyertz, S.; Brown, D. *J. Chem. Phys.* **1996**, *104*, 10063.
(48) Neyertz, S.; Brown, D.; Clarke, J. H. R. *J. Chem. Phys.* **1996**, *105*, 2076.
(49) Neyertz, S.; Brown, D. *J. Chem. Phys.* **2001**, *115*, 708.
(50) Lal, M. *Mol. Phys.* **1969**, *17*, 57.
(51) Metropolis, N.; Rosenbluth, A. W.; Rosenbluth, M. N.; Teller, A. H.; Teller, E. *J. Chem. Phys.* **1953**, *21*, 1087.
(52) Flory, P. J. *The Statistical Mechanics of Chain Molecules*; Hanser Publishers: New York, 1988.
(53) Hofmann, D.; Heuchel, M.; Yampolskii, Y.; Khotimskii, V.; Shantarovich, V. *Macromolecules* **2002**, *35*, 2129.
(54) Brown, D.; Minoux, H.; Maigret, B. *Comput. Phys. Comm.* **1997**, *103*, 170.
(55) Brown, D.; Maigret, B. *Speedup* **1999**, *12*, 33.
(56) Fincham, D. *Mol. Simul.* **1994**, *13*, 1.
(57) Berendsen, H. J. C.; Postma, J. P. M.; Van Gunsteren, W. F.; DiNola, A.; Haak, J. R. *J. Chem. Phys.* **1984**, *81*, 3684.
(58) Brown, D.; Clarke, J. H. R. *Comput. Phys. Commun.* **1991**, *62*, 360.
(59) Knopp, B.; Suter, U. W.; Gusev, A. A. *Macromolecules* **1997**, *30*, 6107.
(60) Knopp, B.; Suter, U. W. *Macromolecules* **1997**, *30*, 6114.
(61) Nick, B.; Suter, U. W. *Comput. Theor. Polym. Sci.* **2001**, *11*, 49.
(62) Widom, B. *J. Chem. Phys.* **1963**, *39*, 2808.
(63) Neyertz, S.; Brown, D.; Douanne, A.; Bas, C.; Albérola, N. D. *J. Phys. Chem. B.* **2002**, *106*, 4617.
(64) Van Krevelen, D. W. *Properties of Polymers: their Correlation with Chemical Structure; their Numerical Estimation and Prediction from Additive Group Contributions*, 3rd completely revised ed.; Elsevier: Amsterdam, 1990.
(65) Hoy, K. L. *J. Paint Technol.* **1970**, *42*.
(66) Fedors, R. F. *Polym. Eng. Sci.* **1974**, *14*, 147.
(67) Zhang, R.; Mattice, W. L. *Macromolecules* **1995**, *28*, 7454.
(68) Kang, J. W.; Choi, K.; Jo, W. H.; Hsu, S. L. *Polymer* **1998**, *39*, 7079.
(69) Kotov, B. V. *Russ. J. Phys. Chem.* **1988**, *62*, 1408.
(70) LaFemina, J. P.; Arjavalingam, G.; Houghman, G. *J. Chem. Phys.* **1989**, *90*, 5154.
(71) Salley, J. M.; Frank, C. W. In *Polyimides: Fundamentals and Applications*; Ghosh, M. K., Mittal, K. L. Eds.; Marcel Dekker: New York, 1996; p 279.
(72) Dinan, F. J.; Schwartz, W. T.; Wolfe, R. A.; Hojnicki, D. S.; Clair, T. S.; Pratt, J. R. *J. Polym. Sci., Part A: Polym. Chem.* **1992**, *30*, 111.
(73) Ando, S.; Matsuura, T.; Sasaki, S. *Polym. J.* **1997**, *29*, 69.
(74) Wachsman, E. D.; Frank, C. W. *Polymer* **1988**, *29*, 1191.
(75) Viallat, A.; Bom, R. P.; Cohen-Addad, J.-P. *Polymer* **1994**, *35*, 2730.
(76) Koros, W. J.; Paul, D. R.; Rocha, A. A. *J. Polym. Sci., Polym. Phys. Ed.* **1976**, *14*, 687.
(77) Paul, D. R.; Koros, W. J. *J. Polym. Sci., Polym. Phys. Ed.* **1976**, *14*, 675.
(78) Kim, T. H.; Koros, W. J.; Husk, G. R. *Sep. Sci. Technol.* **1988**, *23*, 1611.
(79) Bondi, A. *Physical Properties of Molecular Crystals, Liquids and Gases*; John Wiley & Sons: New York, 1968.
(80) Gusev, A. A.; Suter, U. W.; Moll, D. J. *Macromolecules* **1995**, *28*, 2582.
(81) McQuarrie, D. A. *Statistical Mechanics*; Harper and Row: New York, 1976.
(82) Halgren, T. A. *J. Am. Chem. Soc.* **1992**, *114*, 7827.
(83) Van der Vegt, N. F. A.; Müller-Plathe, F.; Gelessus, A.; Johannsmann, D. *J. Chem. Phys.* **2001**, *115*, 9935.

MA048500Q